IOP PUBLISHING JOURNAL OF PHYSICS: CONDENSED MATTER
J. Phys.: Condens. Matter **23** (2011) 455902 (6pp) doi:10.1088/0953-8984/23/45/455902

Ab initio study of magnetoelectricity in Fe/$BaTiO_3$: the effects of n-doped perovskite interfaces

M Hölzer[1], M Fechner[2], S Ostanin[1] and I Mertig[1,3]

[1] Max-Planck-Institut für Mikrostrukturphysik, Weinberg 2, D-06120 Halle, Germany
[2] Department of Materials, ETH Zürich, Wolfgang-Pauli-Straße 27, 8093 Zürich, Switzerland
[3] Institut für Physik, Martin-Luther-Universität Halle-Wittenberg, D-06099 Halle, Germany

E-mail: mhoelzer@mpi-halle.de

Received 8 August 2011, in final form 16 September 2011
Published 28 October 2011
Online at stacks.iop.org/JPhysCM/23/455902

Abstract
On the basis of *ab initio* calculations we study the interfacial magnetoelectric effect in a prototypical biferroic $Fe_L/XO_2/BaO/BaTiO_3(001)$ (X = Ti, V, Co), with an Fe thickness $L \leq 2$ monolayers. We anticipate that the use of the n-type perovskite termination instead of nominally neutral TiO_2 may enhance magnetoelectricity in the system when its magnetization is robustly changed by substrate-polarization reversal.

(Some figures may appear in colour only in the online journal)

1. Introduction

Currently, many research laboratories across the world are focusing on controlling the magnetic state of materials by the use of an electric field. Multiferroic (MF) oxides, i.e. materials where ferroelectricity and ferromagnetism coexist [1], in principle, allow a switchable magnetization [2]. Since the electric field, **E**, applied to a MF displaces its magnetic ions this affects the magnetic exchange coupling and changes the magnetization: $\mu_0 \Delta M_i \sim \alpha_{ij} E_j$, where α_{ij} is the magnetoelectric (ME) tensor and $(i, j) = x, y, z$. This phenomenon may allow us to store information in nanometer-sized logic memories [3, 4]. For bulk MFs, the obtained ME coupling is usually weak [5, 6]. There are a few exceptions [7], such as $TbMnO_3$, but their ferroelectricity is caused by a particular type of magnetic order, which exists only at low temperatures and which is mostly antiferromagnetic.

Another rapidly developing mainstream idea in the field of MFs is based on the use of interfacial ME coupling which can occur between a ferroelectric and a strong ferromagnet. For the ferromagnetic component of a composite MF, significant changes in the interfacial magnetization and spin polarization are anticipated in response to a ferroelectric polarization reversal [8–11]. The interface ME effect is formally defined [8] at the coercive field E_c: $\mu_0 \Delta M \sim \alpha E_c$. Thus, the parameter α determines the change of the ferromagnet's magnetization under polarization reversal in the ferroelectric component. Recently, controlled spin polarization through an interfacial ME has been demonstrated by ferroelectric tunnel junctions with ferromagnetic leads [12]. In this context, the interface between Fe and $BaTiO_3$ (BTO) represents an archetypal system in which the commonly used ferroelectric is combined with a ferromagnetic electrode in an almost perfect lattice match (misfit 1.4%). So far our knowledge of composite MFs is limited to the *ab initio* based predictions, while quantitative information on growth of the thickness-dependent geometric structures and interfaces is not available.

For a single Fe monolayer (ML) on BTO, theory predicts [9, 13] that interfacial ME coupling alters the magnetocrystalline anisotropy energy by ~50%. The magnetization of Fe/BTO can be tuned to almost zero upon deposition of a second Fe ML. Ferromagnetic order is restored for Fe films thicker than $L = 3$ MLs where the shape anisotropy energy favors the in-plane easy axis [13]. Until recently, calculations for composite MFs were focused on chemically perfect interfaces with no impurities. However, the occurrence

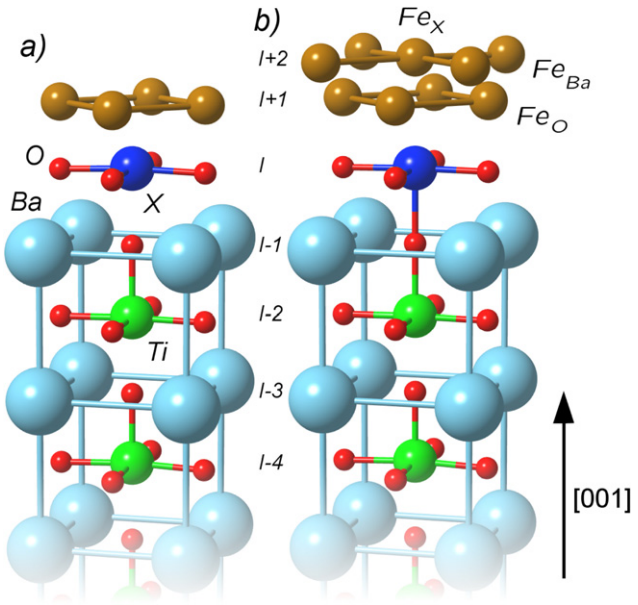

Figure 1. Top layers of the $(Fe_2)_L/XO_2/BaTiO_3(001)$ unit cell are shown for $L = 1$ and $L = 2$ in panels (a) and (b), respectively. In panel (b), the interfacial Fe atoms above O are marked as 'Fe_O' while the Fe atoms of the second adlayer, which sit above the perovskite cations, are marked with the labels 'Fe_{Ba}' and 'Fe_X'. Graphics produced with VESTA [24].

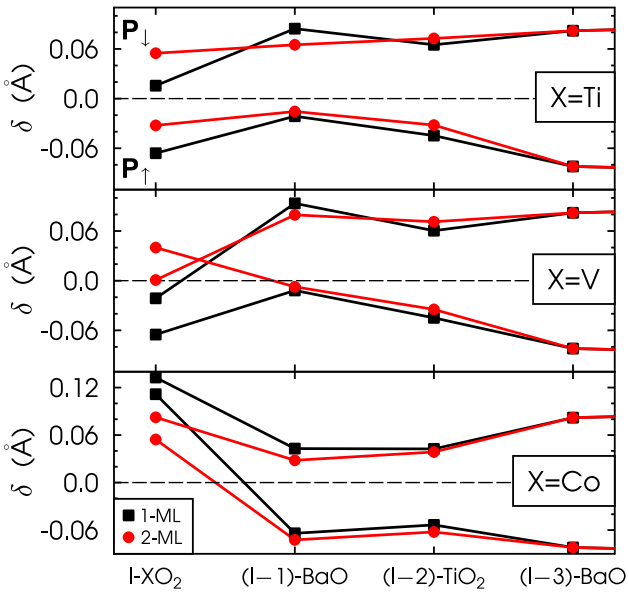

Figure 2. Interlayer displacements $\delta = (z_O - z_{cation})$ (in Å) calculated for the two top perovskite unit cells of $Fe_L/XO_2/BaTiO_3(001)$ ($L = 1, 2$; X = Ti, V, Co and $\mathbf{P} = P_\downarrow, P_\uparrow$). The interfacial XO_2 layer and layers beneath are denoted by **I**, $\mathbf{I} - 1$, $\mathbf{I} - 2$, etc.

of extra oxygen or oxygen vacancies near the biferroic interface may play an important role [15, 16]. The presence of perovskite-cation 3d substitutions at the interface can result in a dramatic change of magnetization under the electric polarization reversal. Recently, the effect of a CrO_2-terminated BTO on magnetoelectricity of $Fe/CrO_2/BTO$ has been computed [17]. In this work, we complete a systematic study of interfacial ME coupling between a thin Fe film and commonly used BTO, with the electron doped termination XO_2 (X = V, Co) instead of nominally neutral TiO_2. The most promising cases of enhanced magnetoelectricity are discussed as well as the magnetization changes induced by polarization reversal.

2. Method

To model the Fe/BTO biferroic system within a slab geometry we used a five-unit-cell thick (∼2 nm) BTO supercell covered by an Fe ML or Fe bilayer ($L = 1, 2$). A 2 nm vacuum layer separates the slabs along [001]. The equilibrium lattice parameters of tetragonal BTO $a = 3.943$ Å and $c/a = 1.013$ were used [14]. For Fe/BTO, the TiO_2-terminated interface is energetically preferred [9]. The opposite surface of the slab is terminated by a BaO layer. Before relaxation, the intralayer perovskite displacements $\delta = (z_O - z_{cation})$ of 0.082 Å and 0.086 Å were fixed in the TiO_2 and BaO layers, respectively. The state $P_\downarrow$ means that $\delta > 0$ and, vice versa, negative δ refers to the state $P_\uparrow$, with the electric polarization pointing parallel to the surface normal. In this work, we substituted an interfacial Ti by V or Co and added one or two MLs of iron on the XO_2-terminated BTO(001). For each substitution and Fe layer thickness, the Fe positions and atomic positions of the two BTO unit cells near the interface were relaxed. The Fe adatoms of the first ML relax atop oxygen [9], while the Fe atoms of the second ML find their relaxed positions above the Ba and X sites. The side views of the $Fe_L/XO_2/BTO(001)$ supercell for $L = 1$ and 2 are shown in figure 1.

We used the Vienna *ab initio* simulation package (VASP) [18, 19] within the local spin-density approximation. The electron–ion interactions were described by projector-augmented wave pseudopotentials [20], and the electronic wavefunctions were represented by plane waves with a cutoff energy of 650 eV. For ionic relaxation an $8 \times 8 \times 4$ k-point Monkhorst–Pack [21] mesh was used. The ionic relaxation was performed until the forces were less than 1×10^{-3} eV Å^{-1}. To calculate the electronic density of states (DOS) we used a $30 \times 30 \times 15$ k-point mesh. For each completely relaxed atomic configuration we performed spin-polarized calculations starting from a ferromagnetic (FM) or, alternatively, from an antiferromagnetic (AFM) configuration in the Fe layers. The induced magnetization of the XO_2 interface was also investigated.

3. Results and discussion

3.1. The structural relaxation

Figure 2 shows the perovskite's δ after relaxation of $Fe_L/XO_2/BTO(001)$ for the interfacial layer **I** and layers beneath. The δ asymmetry seen in figure 2 between $P_\downarrow$ and $P_\uparrow$ as well as the magnitude of δ both mimic the effect of the depolarizing field and its screening. Since the state $P_\downarrow$ is energetically preferable compared to $P_\uparrow$, the depolarization

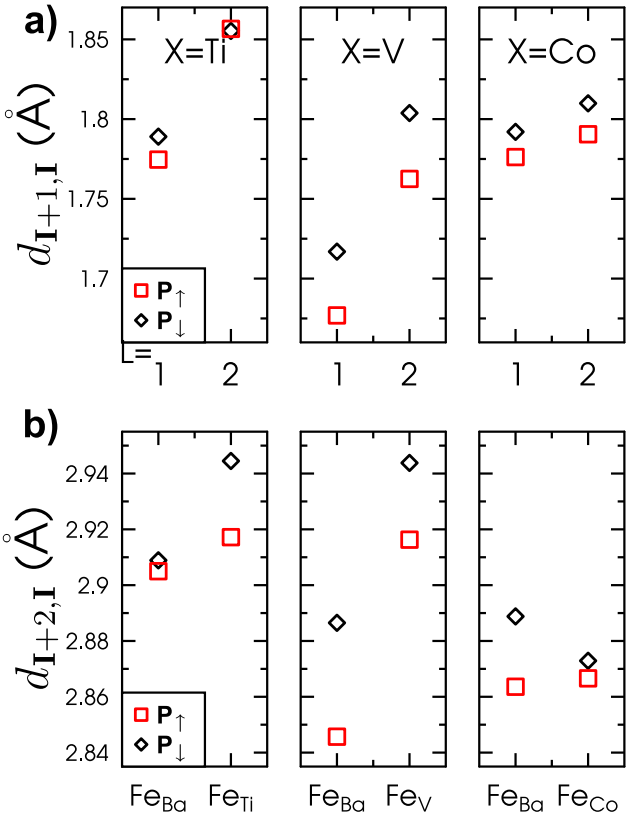

Figure 3. Interlayer distances between Fe-(**I** + 1) and X − **I** (in Å) after relaxation are shown in panel (a) for each X; $L = 1, 2$ and both **P** states. In the case of $L = 2$, the separations between (**I** + 2) and **I** are plotted in panel (b) for each X, each **P** and for the two Fe(**I** + 2) sites above Ba and X.

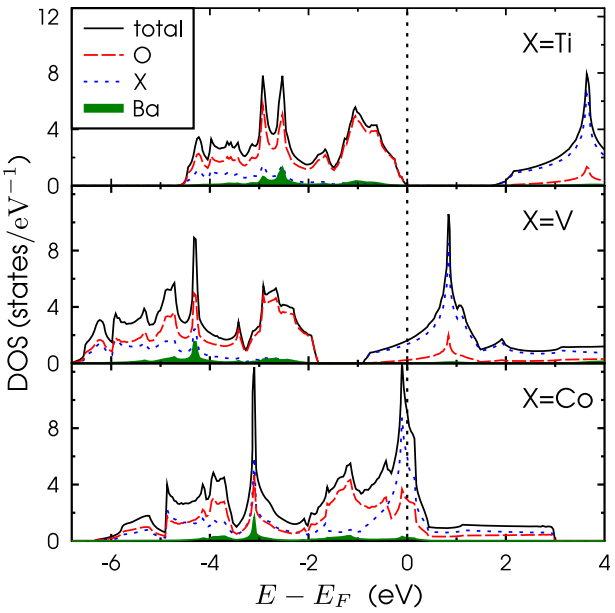

Figure 4. DOS of $BaTiO_3$ compared to that of hypothetical $BaXO_3$ (X = V, Co).

effect should be stronger for $P_\uparrow$. This is shown in figure 2. For nominally neutral X = Ti its δs gradually decrease toward the interface in the case of $P_\uparrow$ while for $P_\downarrow$ the δ value is stable between the layers **I** − 1 and **I** − 3 and, therefore, the reduction of δ becomes crucial at the interface only. For X = V the **I** − δ magnitude increases compared to that of X = Cr but, interestingly, it changes the sign twice: (i) when $L = 2$ and **P** = $P_\uparrow$ and (ii) when $L = 1$ and **P** = $P_\downarrow$. It seems, however, that the largest changes of **I** − δ occur for X = Co, i.e. in the case of which there are five extra electrons at the interface. Here, for both **P** states, all **I** − $\delta > 0$ showing a pronounced increase in magnitude. The latter can indicate structural instability of the system with the CoO_2 perovskite termination.

In figure 3, we plot the relaxed interlayer separations between interfacial Fe and X atoms. The Fe atoms relaxing atop O form a strong and relatively short chemical bond at the interface. When a single Fe adlayer is relaxed on the TiO_2-terminated BTO the Fe atoms find their positions [9] at a distance of 1.78 Å as shown in panel (a) of figure 3. For X = Ti, $d_{I+1,I}$ increases by ∼5% when the second Fe ML is added while the polarization reversal shows no effect on $d_{I+1,I}$. For any perovskite interface with excessive electrons, its $d_{I+1,I}$ shown in figure 3(a) is significantly reduced compared to the Fe/TiO_2/BTO system. In particular, for $L = 1$ and X = V, we find that $d_{I+1,I} \approx 1.7$ Å. When the second Fe layer is added above VO_2, despite the ∼5% increase of $d_{I+1,I}$, this separation between (**I** + 1) and **I** remains shorter than that of X = Ti. Similarly, the contraction of $d_{I+1,I}$ was obtained for X = Co and $L = 2$ as well. The Fe-(**I** + 2) atoms are placed above the perovskite cations X or Ba. It should be noted that the corresponding Fe_X and Fe_{Ba} sites are environmentally inequivalent. In figure 3(b) we plot the relaxed interlayer separation $d_{I+2,I}$ between the layers **I** + 2 and **I**. In the case of Fe_{Ba}, the n-type interface makes $d_{I+2,I}$ shorter than the reference X = Ti system but, most importantly, $d_{I+2,I}$ becomes notably changed upon the reversal of **P**. Thus, the structural geometries of composite biferroics with $L = 2$ suggest a promising scenario of tunable magnetization by electric polarization reversal. Figure 3 also tells us about the interlayer distance of the Fe bilayer for $L = 2$. The average value lies in the range 1.07–1.08 Å.

3.2. The electronic and magnetic properties

The site-projected DOS of paraelectric cubic $BaTiO_3$ are shown in figure 4 together with the DOS of hypothetical cubic $BaXO_3$ (X = V, Co). All perovskite systems were calculated using the same lattice parameter $a = 3.943$ Å. For BTO we obtained a band gap of ∼2 eV, which is typically underestimated within the standards of the local density approximation. The conduction band of BTO is formed mainly by the Ti 3d states whereas the upper valence band is largely composed of O 2p states. In $BaXO_3$ (X = V, Co), the DOS is typically metallic while the 3d states of X species dominate near the Fermi level, E_F. For X = V there is a ∼1 eV pseudogap seen at −1.5 eV below E_F, which finally closes in $BaCoO_3$. Thus, one can expect relatively strong metallization at the Fe/XO_2 interface compared to Fe/TiO_2.

Table 1. Local magnetic moments (in μ_B) calculated for the two Fe adlayers labeled by $\mathbf{I}+1$ and $\mathbf{I}+2$ and interfacial X (X = Ti, V, Co) and O of $Fe_L/XO_2/BaTiO_3(001)$ ($L = 1, 2$). In the topmost Fe layer, $\mathbf{I}+2$, there are two inequivalent sites denoted as Fe_{Ba} and Fe_X. The total magnetization M_{tot} (in μ_B) includes additional contributions from the interstitials. The energy difference $\Delta E = E_{AFM} - E_{FM}$ (in eV/cell) between the AFM and FM configurations calculated for each system at $\mathbf{P} = (P_\uparrow, P_\downarrow)$ is shown as well as the interfacial ME coupling α (in 1×10^{-10} G cm^2 V^{-1}).

Site	Layer	**P**	X = Ti		X = V		X = Co	
			$L=1$	$L=2$	$L=1$	$L=2$	$L=1$	$L=2$
Fe_{Ba}	$(\mathbf{I}+2)$	$P_\uparrow$	—	+2.41	—	+2.31	—	+2.18
		$P_\downarrow$	—	+2.36	—	+2.37	—	+2.18
Fe_X	$(\mathbf{I}+2)$	$P_\uparrow$	—	−2.46	—	−2.66	—	−2.36
		$P_\downarrow$	—	−2.36	—	−2.59	—	−2.26
Fe_O	$(\mathbf{I}+1)$	$P_\uparrow$	+2.83	−0.03	+2.47	+0.19	+2.53	−0.25
		$P_\downarrow$	+2.81	0.00	+2.74	−0.01	+2.41	+0.08
X	$(\mathbf{I})$	$P_\uparrow$	−0.30	0.00	−0.29	−0.28	+0.60	+1.10
		$P_\downarrow$	−0.22	+0.01	−0.98	−0.13	+0.63	−0.06
O	$(\mathbf{I})$	$P_\uparrow$	+0.69	−0.12	+0.04	0.00	+0.12	−0.03
		$P_\downarrow$	+0.75	−0.12	+0.10	−0.01	+0.14	−0.01
M_{tot} (μ_B)	—	$P_\uparrow$	+5.87	+0.02	+5.04	−0.31	+6.02	+0.59
		$P_\downarrow$	+5.84	−0.02	+4.94	−0.42	+5.92	−0.31
ΔE (eV)	—	$P_\uparrow$	+0.69	−0.12	+0.55	−0.12	+0.30	−0.13
		$P_\downarrow$	+0.75	−0.12	+0.59	−0.13	+0.30	−0.13
α (10^{-10} G cm^2 V^{-1})	—	—	2.1	3.1	7.6	7.7	7.3	68

To address the effect of dual polarizability on the metallization and induced magnetization of the BTO termination, we plot the DOS differences between the $P_\uparrow$ and $P_\downarrow$ poled states of $Fe_L/XO_2/BaTiO_3(001)$ for $L = 1$ and 2 in figure 5. The spin-polarized X–DOS curves near the Fermi level, namely between -0.2 eV $< E_F < 0.2$ eV, are shown there. For the TiO_2 interface, a prominent effect seen in figure 5 in the minority-spin Ti–DOS at $E = E_F$ illustrates the charge transfer occurring at the biferroic interface due to the **P** reversal. Because the Fe–Ti separation is shorter for $P_\downarrow$ than for $P_\uparrow$, the overlap between the Fe and Ti d orbitals is larger, leading to the excessive electrons which result in slightly larger magnetic moments.

All magnetic moment values of the system are collected in table 1 together with the energy difference $\Delta E = E_{AFM} - E_{FM}$ between the AFM and FM configurations for each **P**. We consider, firstly, the case $L = 1$. Here, the FM order is energetically favorable against the AFM solution for all X species. In $Fe_{L=1}/TiO_2/BTO$ the FM order is preferable by 0.7 eV/cell (0.75 eV/cell) for $P_\uparrow$ ($P_\downarrow$) with the Fe and O magnetic moments being aligned parallel whereas the Ti magnetic moment, which originates from hybridization of the Ti 3d and Fe 3d minority states, is antiparallelly aligned. For X = Ti, the polarization reversal from $P_\downarrow$ to $P_\uparrow$ yields a magnetization change of $|\Delta M| = 0.028\ \mu_B$/cell which formally results in the ME coupling of 2.1×10^{-10} G cm^2 V^{-1}. All α values have been calculated using an assumed coercive field of $E_c = 10$ kV cm^{-1}. When Ti is substituted by V at the interface, the lowest-energy magnetic configuration for $L = 1$ remains ferromagnetic. However, the larger negative magnetic moment induced on V for $P_\downarrow$ yields the larger value of α. In the case of Cr, the m_{Cr} magnetic moments are much larger than m_{Ti}, while the calculated magnetic moment of interfacial oxygen is about

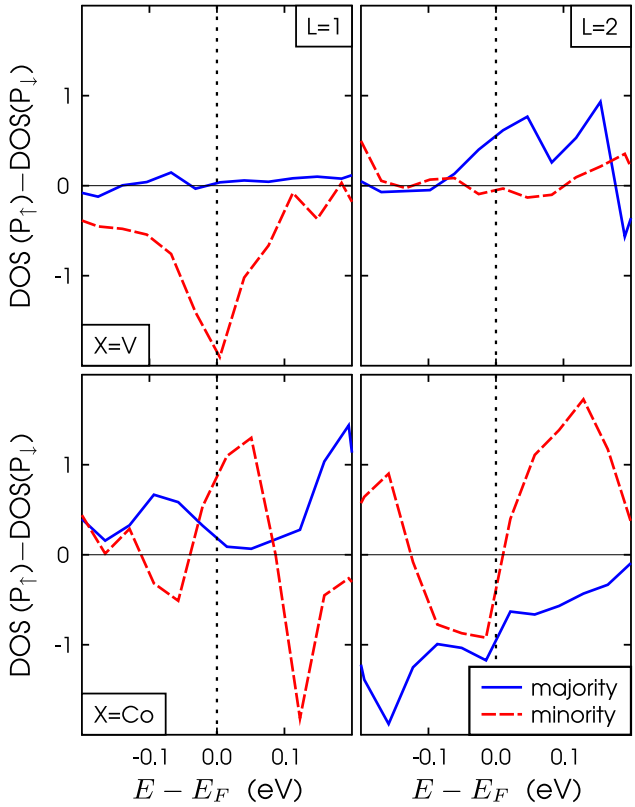

Figure 5. Spin-polarized X-projected DOS differences calculated between the $P_\uparrow$ and $P_\downarrow$ states of $Fe_L/XO_2/BaTiO_3(001)$ for $L = 1, 2$.

0.1 μ_B. This value as well as m_{Cr} are in good agreement with the experimental data for bulk CrO_2. Due to the large and negative Cr magnetic moment, the total magnetization of the system $Fe_{L=1}/CrO_2/BTO$ is reduced by $\approx 2\ \mu_B$ in comparison

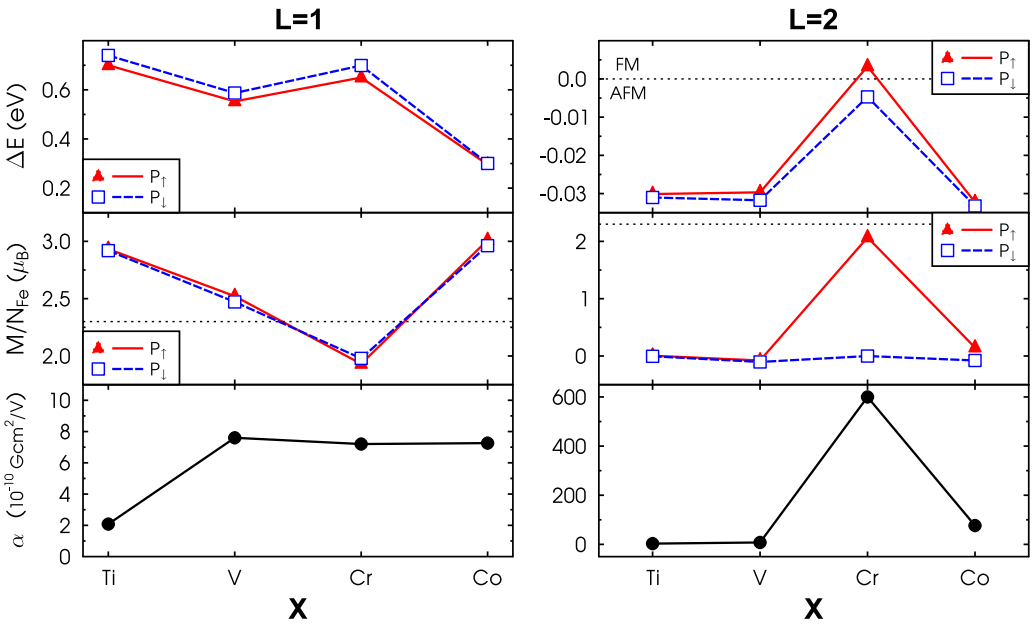

Figure 6. ME properties of $Fe_L/XO_2/BaTiO_3(001)$ ($L = 1, 2$). The top panel shows the energy difference $\Delta E = E_{AFM} - E_{FM}$ for each X and for both $P_\uparrow$ and $P_\downarrow$. The middle panel shows the total magnetization, normalized by the number of Fe atoms per unit cell. The dashed line indicates the magnetic moment of bulk Fe as a reference. The ME figure of merit α is plotted in the bottom panel.

to that of $Fe_{L=1}/TiO_2/BTO$. Although m_{Cr} is moderately changed by the **P** reversal, the corresponding $|\Delta M|$ results in $\alpha = 7.2 \times 10^{-10}$ G cm^2 V^{-1} which is three times larger than the ME effect of $Fe_{L=1}/TiO_2/BTO$. For $Fe_{L=1}/CoO_2/BTO$, we find that its α is compatible to that of X = Cr.

For the Fe bilayer on BTO, there are two environmentally inequivalent **I** + 2 sites situated atop Ba and Ti, respectively, which are labeled by Fe_{Ba} and Fe_X in figure 1. The different magnetic moments of the Fe-(**I** + 2) atoms shown in table 1 reflect their atomic volumes and hybridization of the electronic states. For X = Ti, the value of m_{Fe} in the layer **I** + 1 is almost quenched while the two sizable moments in the surface layer **I** + 2 are aligned antiparallel. This results in $M \to 0$ for $Fe_{L=2}/TiO_2/BTO(001)$. For X = V and Co the calculated magnetic moments and their variation with Fe film thickness and reversal of **P** tend to be similar to that of X = Ti.

We plot the energy difference $\Delta E = E_{AFM} - E_{FM}$ normalized per Fe atom and calculated for $L = 1$ and 2 in figure 6. For comparison, we included the results from [17] for X = Cr, where the Fe bilayer represents a specific case of a magnetically soft system. This is shown in the top panel of figure 6. Here, the magnetic order can be switched by the **P** reversal from ferromagnetic to antiferromagnetic while the total magnetization of the system is also changed by $\sim 2\ \mu_B$ per Fe as shown in the middle panel of figure 6; therefore, the ME coupling coefficient is largely enhanced. It should be noted that this potentially attractive magnetic switch upon the reversal of **P** requires an electric field which exceeds the coercive field value of BTO.

A similar behavior was recently found for Fe islands on a Cu(111) surface, where the magnetic ordering can be switched from FM to AFM by application of an electric field [23].

4. Conclusions

In summary, we have presented an *ab initio* study of the effect of interfacial 3d substitutions on the strength of ME coupling seen in composite biferroics $Fe_L/XO_2/BaTiO_3(001)$, with Fe of thickness $L \leq 2$ MLs. We demonstrated that the use of the n-type terminated perovskite interface instead of nominally neutral TiO_2 may significantly enhance magnetoelectricity in the system. Nevertheless, the observed effect is smaller than in the case of X = Cr, published in [17].

Acknowledgment

This work was supported by the Collaborative Research Network SFB 762, 'Functionality of Oxidic Interfaces'.

References

[1] Wang K F, Liu J-M and Ren Z F 2009 *Adv. Phys.* **58** 321
[2] Lottermoser T 2004 *Nature* **430** 541
[3] Eerenstein W, Wiora M, Prieto J L, Scott J F and Mathur N D 2007 *Nature Mater.* **6** 348
[4] Zavaliche F, Zhao T, Zheng H, Straub F, Cruz P, Yang P-L, Hao D and Ramesh R 2007 *Nano Lett.* **7** 1586
[5] Ederer C and Spaldin N A 2005 *Curr. Opin. Solid State Mater. Sci.* **9** 128
[6] Picozzi S and Ederer C 2009 *J. Phys.: Condens. Matter* **21** 303201
[7] Khomskii D 2009 *Physics* **2** 20
[8] Duan C-G, Jaswal S S and Tsymbal E Y 2006 *Phys. Rev. Lett.* **97** 047201
[9] Fechner M, Maznichenko I V, Ostanin S, Ernst A, Henk J, Bruno P and Mertig I 2008 *Phys. Rev.* B **78** 212406

[10] Fechner M, Maznichenko I V, Ostanin S, Ernst A, Henk J and Mertig I 2010 *Phys. Status Solidi* b **247** 1600
[11] Burton J D and Tsymbal E Y 2009 *Phys. Rev.* B **80** 174406
[12] Ramesh R 2010 *Nature Mater.* **9** 380
[13] Duan C-G, Velev J P, Sabirianov R F, Mei W N, Jaswal S S and Tsymbal E Y 2008 *Appl. Phys. Lett.* **92** 122905
[14] Fechner M, Ostanin S and Mertig I 2008 *Phys. Rev.* B **77** 094112
[15] Niranjan M K, Velev J P, Duan C-G, Jaswal S S and Tsymbal E Y 2008 *Phys. Rev.* B **78** 104405
[16] Fechner M, Ostanin S and Mertig I 2009 *Phys. Rev.* B **80** 094405
[17] Hölzer M, Fechner M, Ostanin S and Mertig I 2010 *Phys. Rev.* B **81** 214428
[18] Kresse G and Hafner J 1994 *Phys. Rev.* B **49** 14251
[19] Kresse G and Furthmüller J 1996 *Phys. Rev.* B **54** 11169
[20] Kresse G and Joubert D 1999 *Phys. Rev.* B **59** 1758
[21] Monkhorst H J and Pack J D 1976 *Phys. Rev.* B **13** 5188
[22] Leung T, Chan C and Harmon B 1991 *Phys. Rev.* **44** 2923
[23] Gerhard L *et al* 2010 *Nature Nanotechnol.* **5** 792–7
[24] Momma K and Izumi F 2008 *J. Appl. Crystallogr.* **41** 653–8